

RESEARCH

Open Access



# Correlation study on firing temperature and color of plain pottery excavated from the Tang Dynasty tomb of Liu Jing in Shaanxi, China

Biao Zhang<sup>1</sup>, Hang Wang<sup>1</sup>, Xuanliang He<sup>1</sup>, Jianfeng Zhu<sup>1</sup>, Hongjie Luo<sup>1,2</sup>, Daiyun Liu<sup>3</sup>, Fen Wang<sup>1</sup>, Xichen Zhao<sup>3</sup>, Guiqiang Fei<sup>4</sup> and Pei Shi<sup>1\*</sup>

## Abstract

Plain pottery excavated from the Tang Dynasty tomb of Liu Jing was taken as the research object. The color, chemical composition, microstructure, and phase were tested to investigate the influencing factors of color for plain pottery fragments. The results indicated that the contents of  $\text{Fe}_2\text{O}_3$  and  $\text{TiO}_2$  in all fragments varied little, and the influence of humic acids in clay as well as the firing atmosphere on the appearance color of plain pottery was excluded. Therefore, the main factor affecting color saturation ( $C^*$ ) was identified as the firing temperature ( $T$ ). More importantly, the correlation between  $C^*$  and firing temperature was established by replicas fired at different temperatures. Before the appearance of the glass phase, iron-containing minerals played a major role in coloring, and after that, iron ions in the glass phase and iron crystallization rose the important function of coloring. Consequently, with the increase of firing temperature,  $C^*$  value increased firstly and then decreased. The inflection point of the fitted  $C^* - T$  curve corresponded to the glass phase formation temperature. By comparing the estimated firing temperatures obtained by the fitted  $C^* - T$  correlation curve with the known firing temperature of replicas, it was demonstrated that the color measurement is an ideal method for deducing the firing temperatures of ancient plain pottery.

**Keywords** Plain pottery, Firing temperature, Color saturation, Iron-containing minerals, Replica

## Introduction

There are numerous pottery cultural relics excavated from ancient tombs in China. They are the witnesses and physical carriers of thousands of years of history and civilizations, and have extremely high historical, artistic, and scientific values. However, under the influence of natural and human factors, pottery cultural relics have serious diseases, such as cracks and fragments, which are closely related to their mechanical properties [1, 2]. To a certain extent, the firing temperature decides the density of the pottery and thus affects its mechanical properties [3]. At the archaeological excavation site, there are diverse extraction methods for pottery fired at different temperatures. Generally, it could be extracted directly for high-temperature pottery, while it needs to be temporarily

\*Correspondence:

Pei Shi

shipei7121@163.com

<sup>1</sup> School of Material Science and Engineering, School of Conservation Science and Technology for Cultural Heritage, Key Laboratory of Underground Cultural Relics Conservation Materials and Technology, Ministry of Education, Shaanxi University of Science and Technology, Xi'an 710021, China

<sup>2</sup> Institute for the Conservation of Cultural Heritage, Shanghai University, Shanghai 200444, China

<sup>3</sup> Shaanxi Academy of Archaeology, Xi'an 710043, China

<sup>4</sup> College of Chemistry and Chemical Engineering, Shaanxi University of Science and Technology, Xi'an 710021, China



© The Author(s) 2024. **Open Access** This article is licensed under a Creative Commons Attribution 4.0 International License, which permits use, sharing, adaptation, distribution and reproduction in any medium or format, as long as you give appropriate credit to the original author(s) and the source, provide a link to the Creative Commons licence, and indicate if changes were made. The images or other third party material in this article are included in the article's Creative Commons licence, unless indicated otherwise in a credit line to the material. If material is not included in the article's Creative Commons licence and your intended use is not permitted by statutory regulation or exceeds the permitted use, you will need to obtain permission directly from the copyright holder. To view a copy of this licence, visit <http://creativecommons.org/licenses/by/4.0/>. The Creative Commons Public Domain Dedication waiver (<http://creativecommons.org/publicdomain/zero/1.0/>) applies to the data made available in this article, unless otherwise stated in a credit line to the data.

reinforced firstly and then extracted for low-temperature pottery. Therefore, the determination of firing temperature is essential for the safe extraction and emergency conservation of pottery cultural relics during the excavation process of ancient tombs [4].

At present, the measurement method for the firing temperature of ancient pottery could be roughly divided into two categories. The first is to analyze the shrinkage and expansion characteristics of pottery caused by the phase transition, reaction, or decomposition of raw material components during heating, such as the push-rod thermal expansion method [5]. Nevertheless, its sample preparation process is complex, and the use of the dilatometer to determine the firing temperature of low-temperature pottery (ancient firing temperature is lower than the glass phase formation temperature) is not an ideal method [6–8]. Simultaneously, only the measurement of the densification process by a dilatometer is precise provided that the firing atmosphere is comparable to that of the first firing. The second is to research the change characteristics of specific mineral components in pottery at a certain temperature, such as X-ray diffraction (XRD) [9], simultaneous thermal gravimetric analysis (TGA) [10], Fourier transform infrared spectroscopy (FT-IR) [11] and Raman spectroscopy (Raman) [12]. Although its sample preparation method is simple and the test temperature range is wide, it is also a destructive test. Herein, a non-destructive and rapid detection method of firing temperature is urgently required for the safe extraction and emergency conservation of pottery cultural relics excavated from ancient tombs.

As early as 1971, Matson et al. [13] proposed that the color of pottery was directly related to its firing temperature. But due to the excessive subjectivity of visual color, the method of measuring firing temperature by color had not been widely used. With the continuous development of testing technology, the accuracy and portability of color measuring apparatus are higher and higher, which makes the application of this method possible. Mirti et al. [14] refired the pottery fragments at different temperatures and succeeded in determining the actual firing temperature by analyzing the color changes. Meanwhile, the effect of primary and secondary calcite in the evaluation of the firing temperature of pottery was also studied. It was found that the possibility of correctly estimating firing temperatures may not be affected by CaO contents up to about 5% in a sample fired under oxidizing conditions. Moreover, the error introduced by CaO contents up to 10% may still be comparable with the variation of temperature occurring within an ancient kiln. However, the refiring experiment took a long time and caused damage to the samples. Therefore, it does not meet the

requirements of rapid extraction and emergency conservation of unearthed pottery cultural relics.

In this work, the plain pottery fragments excavated from the Tang Dynasty tomb of Liu Jing in the 12th year of Zhenguan (638 AD) were obtained from Shaanxi Academy of Archaeology. Through the analysis of color, chemical composition, microstructure, and phase, the relationship between color and firing temperature of plain pottery fragments was determined, and the influence mechanism of firing temperature on the color of plain pottery was also studied. To verify the reliability of the relationship between color and firing temperature, the samples were fired at different temperatures by the loess from Yaozhou kiln site and the eastern mausoleum of Qin Dynasty in Shaanxi Province, respectively. This work not only provided a theoretical basis for the rapid determination of the firing temperature of plain pottery cultural relics, but also provided a scientific basis for the on-site extraction and emergency conservation of pottery cultural relics excavated from ancient tombs.

## Experimental

### Sample descriptions

From November to December 2020, a Tang Dynasty tomb was excavated by Shaanxi Academy of Archaeology in Buli Village, Dizhang Street, Xianyang City. According to the unearthed epitaph, the tomb owner is Liu Jing who lived in the 12th year of Tang Zhenguan (638 AD). Thirty-two fragments of plain pottery excavated from the tomb of Liu Jing are selected and shown in Fig. 1. According to the different types and parts, they were divided into three categories: nine pottery figurines, twelve pottery horse legs, and eleven pottery horse bodies. Among them, the overall hardness of the pottery figurine was low; the pottery horse leg was relatively firm due to the fixation of iron wires, but there were many cracks; the pottery horse body was porous and fragile.

### Characterization

Chroma values ( $L^*$ ,  $a^*$ ,  $b^*$ ,  $C^*$ ,  $h^*$ ) were obtained with an X-Rite Ci7800 colorimeter and a white standard as reference. X-ray fluorescence (XRF) was operated using a spectrometer from HORIBA XGT-7200, at 50 kV and 1 mA, with a beam size of 1.2 mm diameter. XPS analysis was carried out using an AXIS Supra photoelectron spectrometer equipped with an Al  $K\alpha$  radiation. X-ray diffraction (XRD) patterns of powder samples were obtained by a Rigaku Smart Lab 9 kW diffractometer, using Cu  $K\alpha$  radiation, operating at 40 kV and 100 mA. The step speed was 8 °C/min and the step interval was 0.02°. Optical images of the sample surface were performed using a KEYENCE optical microscope equipped

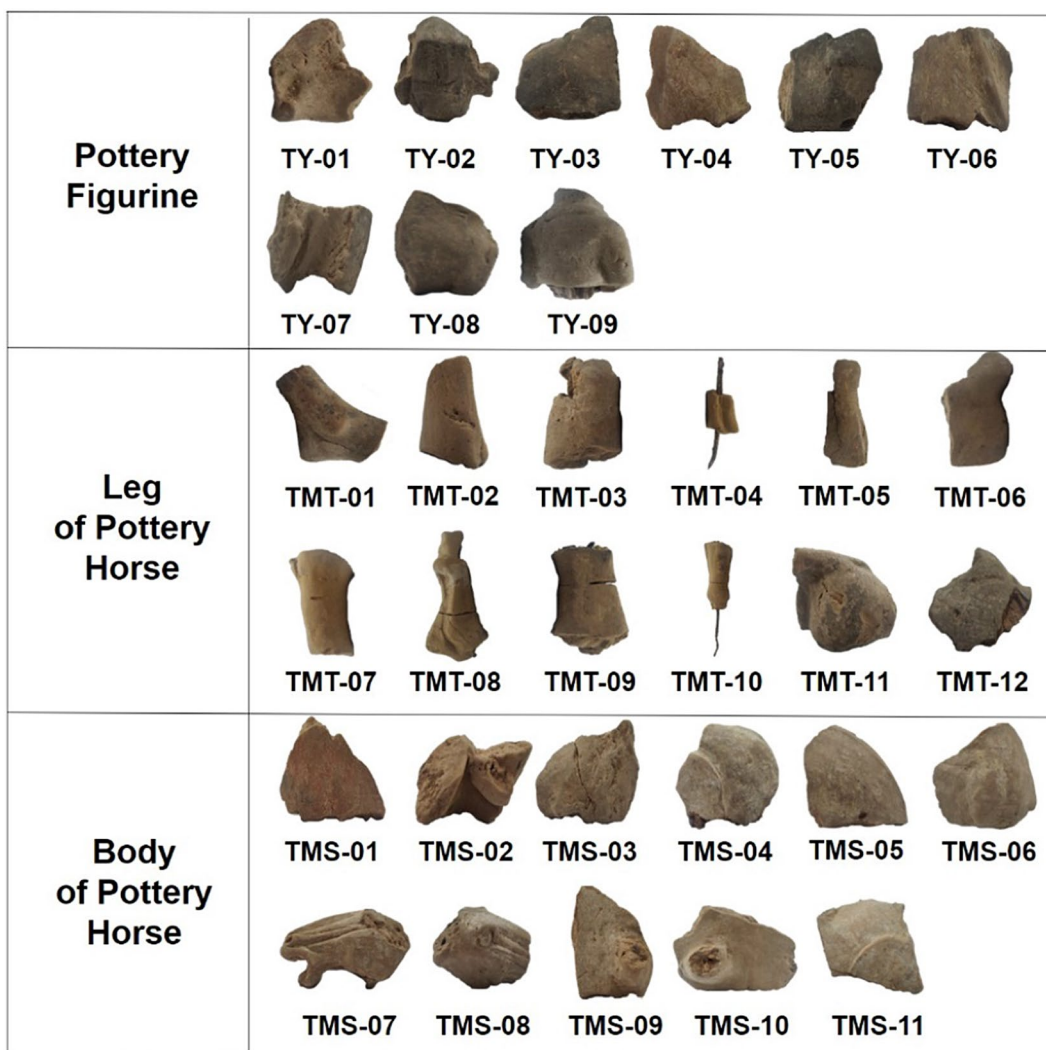


**Fig. 1** Photos of thirty-two plain pottery fragments from the Tang Dynasty tomb of Liu Jing

with a surface depth observation system (VHX-7000). The pore size distribution and porosity of samples were measured by the mercury intrusion method. Hysteresis loops of powder samples at room temperature were performed on a LakeShore 7404 vibrating sample magnetometer (VSM) with a maximum applied field of 2.17 T. The hysteresis parameters saturation magnetization ( $M_s$ ), saturation remanent magnetization ( $M_{rs}$ ) and coercive force ( $B_c$ ) were determined by hysteresis loops.

Micro-Raman spectra of the sample surface were performed using the Renishaw inVia spectrometer. The laser spot size was around 2–3  $\mu\text{m}$  diameter. Laser power of 1 mW at  $\times 50$  magnification was employed to analyze crystals on the pottery surface. The thermal expansion curve was carried out by the NETZSCH DIL402 thermodilatometer with the sample size of

25  $\times$   $\phi$  5 mm, the heating rate of 10  $^\circ\text{C}/\text{min}$ , and purge gas of nitrogen at flow rate of 50 mL/min. The total humic acids in samples were determined by the Agricultural Industry Standard of the People’s Republic of China (NY/T 1867–2010). The content of humic acids is measured by mass fraction, the value is expressed in milligrams per kilogram (mg/kg or ppm), and calculated according to Eq. 1:

$$X_0 = \frac{0.003(V_0 - V)c}{m} \tag{1}$$

where  $V_0$  is the volume of ferrous sulfate standard solution consumed during the blank test, and the unit is milliliters (mL);  $V$  is the volume of ferrous sulfate standard solution consumed for sample determination, in milliliters (mL);  $c$  is the concentration of ferrous sulfate standard

solution, in moles per liter (mol/L); 0.003 is the millimolar mass of 1/4 carbon atom, in grams per mole (g/mol), and  $m$  is the mass of the powder sample, in grams (g).

### Results and discussion

The chroma values of the plain pottery fragments are given in Additional file 1: Table S1. The variation ranges of  $L^*$  of the pottery figurines, pottery horse legs and pottery horse bodies were similar, 45–59, 49–62, and 51–59, respectively. However, the  $a^*$  and  $b^*$  values varied widely, causing the values of  $C^*$  and  $h^*$  to vary between 14–32 and 60°–72°. In order to analyze the variation law deeply, the polar diagram of  $C^*$  and  $h^*$  is shown in Fig. 2. For

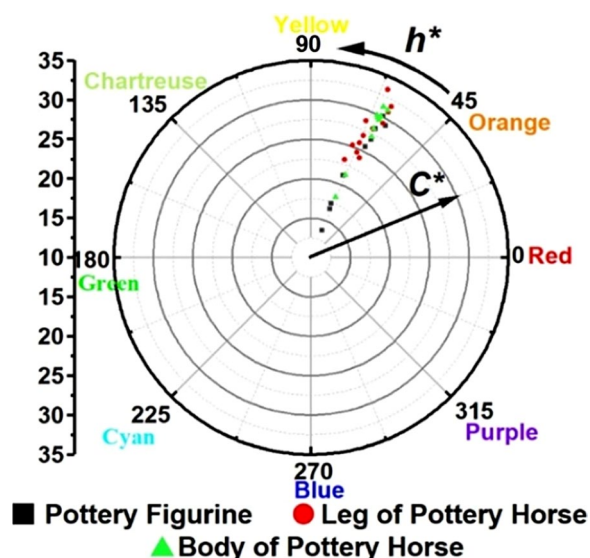


**Fig. 2** Polar diagram of  $C^*$  and  $h^*$  for thirty-two plain pottery fragments

all plain pottery fragments, the angular distribution of the color points had little change, concentrating in the orange-yellow area, and the radial change was obvious. It was indicated that the difference between their colors was mainly reflected in  $C^*$ , not in  $h^*$  [15]. Moreover, it was indicated that the firing atmosphere of plain pottery could be the same because of the very narrow distribution of  $h^*$ .

Redox balances are a function of both the atmosphere ( $\text{CO}/\text{CO}_2$  and  $\text{H}_2/\text{H}_2\text{O}$  balance) and also the presence of carbon in the dough which leads to the formation of C and CO. Because the raw material for pottery is clay, which contains very little carbon content, it has little impact on the redox balance. Hence, the main impact is still the firing atmosphere. To determine the firing atmosphere of the thirty-two plain pottery fragments from the Tang Dynasty tomb of Liu Jing, high-resolution XPS spectra of Fe 2p region (700–735 eV) for the surface and core of TMS-08 were conducted, as shown in Fig. 3. Fe 2p region for Fe 2p<sub>3/2</sub> and Fe 2p<sub>1/2</sub> showed double peaks around 710.3 and 724.5 eV. The binding energy values were consistent with typical values observed for Fe<sub>2</sub>O<sub>3</sub> [16]. The two satellite peaks were observed at approximately 712.8 and 718.2 eV, most likely indicating the presence of Fe<sup>3+</sup> species [17]. In addition, the XPS spectra on the surface and core are not significantly different, indicating that their use and burial have little impact on the color.

The main factors affecting  $C^*$  of pottery include the mineral composition of clay, the chemical composition of products, and firing temperature [18]. Humic acids, as one of the mineral components of clay, often make the clay appear dark or even black. In order to verify the effect of humic acids content in clay on the color of plain pottery, the loess from Yaozhou kiln site was used

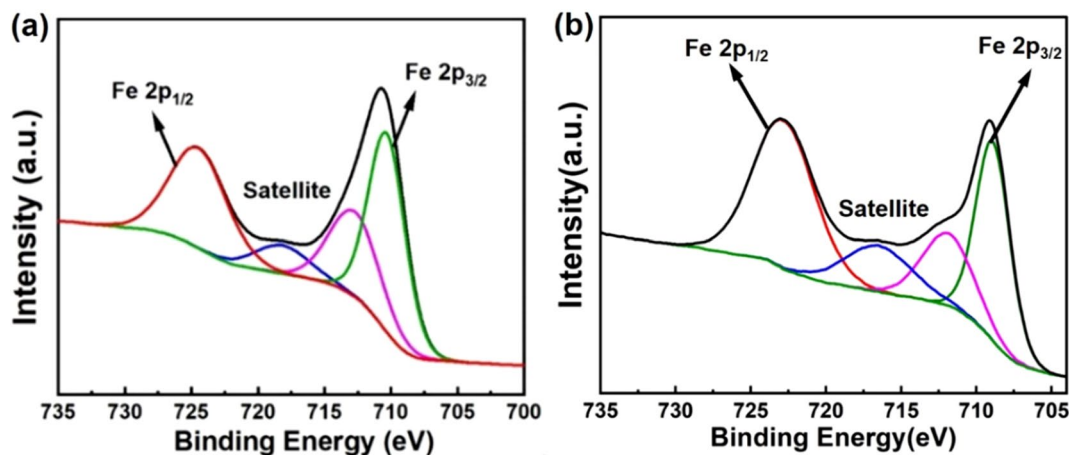


**Fig. 3** XPS high-resolution spectra of Fe 2p for the surface (a) and core (b) of TMS-08

as raw material, and pressed into cake-like bodies of  $\phi$  2 cm. The green bodies were fired by a muffle furnace at 600, 800, and 1000 °C under an oxidizing atmosphere to obtain the replicas. The total humic acids in samples were determined according to NY/T 1867–2010. The technical parameters and calculation results of humic acids content during determination are shown in Table 1. It can be seen that the content of humic acids in the unfired sample is relatively high (4122.23 ppm), while the content of humic acids in the sample fired at 600 °C decreases sharply (only 0.58 ppm), indicating that the humic acids have been basically decomposed at 600 °C. The content of humic acids in the sample fired at 800 °C and 1000 °C is none, indicating that the humic acids have been completely decomposed at these two temperatures, which is consistent with the results reported in the literature [19, 20]. Therefore, the effect of humic acids on the color of plain pottery does not need to be considered. Additional file 1: Table S2 shows the chemical compositions of plain pottery fragments measured by XRF. The contents of all elements were basically constant, indicating that the source and proportion of raw materials were relatively stable. The similar firing atmosphere, stable source and proportion of raw materials proved that the plain pottery excavated from the Tang Dynasty tomb of Liu Jing might have been fired in the same kiln.

In the chemical composition of plain pottery, the coloring element has a remarkable influence on its coloring. Based on Additional file 1: Table S2, the contents of  $\text{Fe}_2\text{O}_3$  and  $\text{TiO}_2$  in different plain pottery fragments were analyzed. As shown in Fig. 4, they varied little. Therefore, for the plain pottery fragments excavated from the tomb of Liu Jing, the factor affecting  $C^*$  was not the chemical composition, but the firing temperature. In order to study the influence of firing temperature on  $C^*$  of the plain pottery fragments, TMS-07, TMS-08, and TMS-09 were selected for in-depth analysis based on the test data in Additional file 1: Tables S1 and S2.

Figure 5 displays the optical micrographs of TMS-07, TMS-08, and TMS-09 and the corresponding three-dimensional microstructures. The comparison revealed that the dark brown irregular patches in the

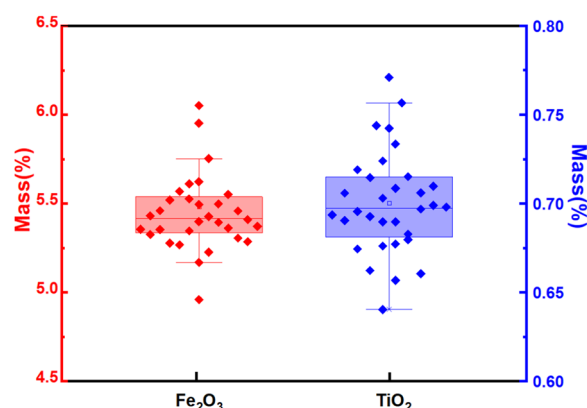


**Fig. 4** Content changes of  $\text{Fe}_2\text{O}_3$  and  $\text{TiO}_2$  in the thirty-two plain pottery fragments

optical micrographs corresponded to the dark blue areas of pores in the 3D microstructure images. Furthermore, the number of pores in TMS-08 was the largest, followed by TMS-07, and TMS-09 the least. Generally, the higher the firing temperature, the denser the microstructure of pottery and the smaller the porosity. From the above micrographs, it can be roughly judged that the firing temperatures of three plain pottery fragments increase in the order of TMS-08, TMS-07, and TMS-09. The measurement results of the porosity and average pore diameter also strongly support this inference (Additional file 1: Fig. S1). In addition to the pores, there were a large number of brownish-yellow bulk crystals and translucent bulk crystals, as well as a small amount of black lamellar crystals and reddish-brown reniform crystals on the surface of the samples.

The XRD patterns of TMS-07, TMS-08, and TMS-09 are shown in Fig. 6a. The characteristic peaks of quartz, anorthite, plagioclase, calcite, and mica minerals (illite and muscovite) were recorded in every pottery fragment. Feldspar minerals start to melt above 1000 °C [9]. The melting temperature range of mica minerals is 850–950 °C, and the thermal decomposition of calcite is started at approximately 750–850 °C [21]. In addition, comparing the diffraction peak intensity of samples,

**Table 1** The technical parameters and calculation results of humic acids content in replicas

Sample	The volume of ferrous sulfate standard solution consumed during blank test ( $V_0$ /mL)	The volume of ferrous sulfate standard solution consumed for sample determination ( $V$ /mL)	The concentration of ferrous sulfate standard solution ( $c$ / mol/L)	The mass of the powder sample ( $m$ / g)	The content of humic acids ( $X_f$ /ppm)
Unfired	49.17	44.68	0.1	0.3269	4120.53
Firing at 600 °C	49.17	48.54	0.1	0.3276	0.58
Firing at 800 °C	49.17	49.17	0.1	0.3286	0
Firing at 1000 °C	49.17	49.17	0.1	0.3808	0

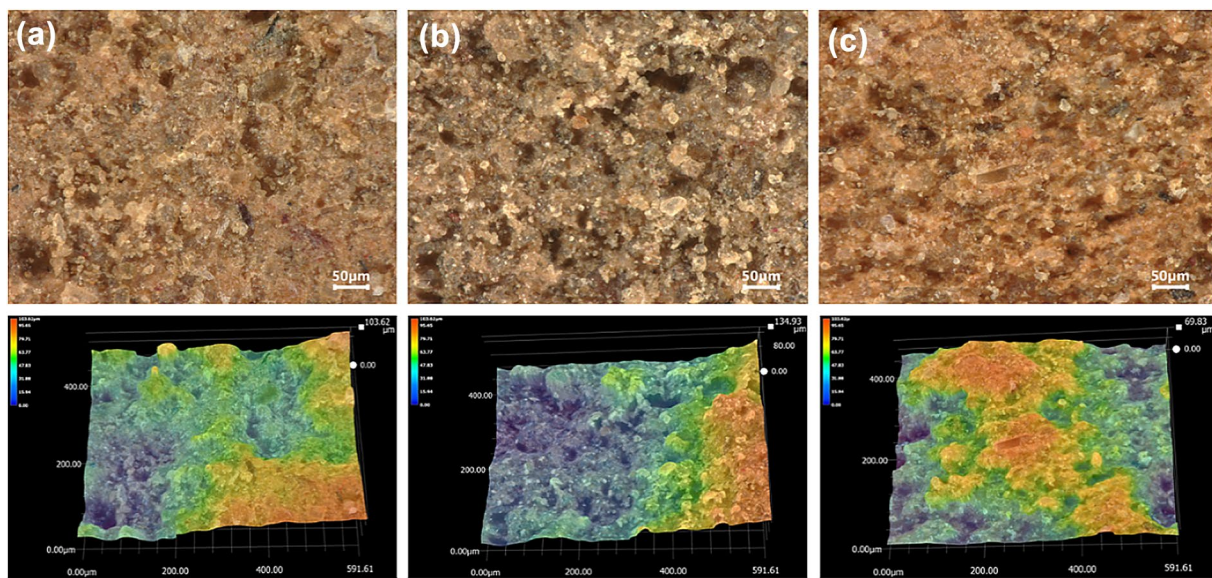


**Fig. 5** Optical micrographs of TMS-07, TMS-08, and TMS-09 (a–c) and corresponding three-dimensional micrographs under  $\times 500$

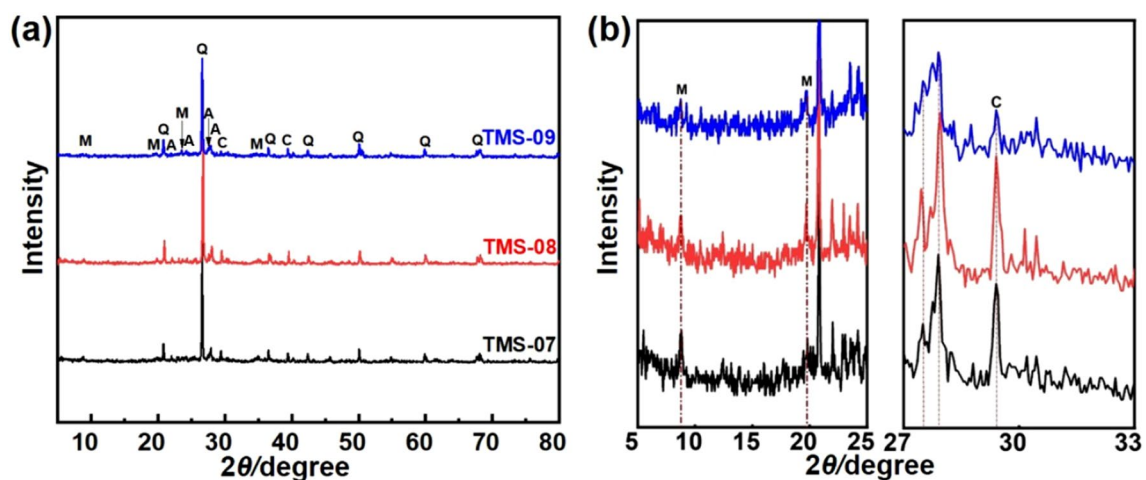


**Fig. 6** XRD patterns (a) and local enlarged drawing (b) of TMS-07, TMS-08, and TMS-09 (Q Quartz; A Anorthite; M Muscovite and illite; P Plagioclase; C Calcite)

quartz and feldspar minerals were not much different, but mica minerals and calcite had differences (Fig. 6b). TMS-08 was the strongest, TMS-07 was in the middle, and TMS-09 was the weakest. The results indicated that the firing temperature increases in the order of TMS-08, TMS-07, and TMS-09. Besides, TMS-08 was fired at less than 750 °C, TMS-07 was fired at 750–850 °C, and TMS-09 was fired at 850–950 °C.

Even though the detected minerals were known as white or clear colors, iron oxide, mineralogical factors that induce brownish or blackish colors, were not detected among the soil component materials. In

particular, the iron oxides in the soil exist as nano-sized particles that cover individual soil particles and have a low crystallinity.

Hysteresis loops were used to infer the type of iron oxide crystals by analyzing the magnetic domain structure of magnetic minerals. The hysteresis loops of TMS-07, TMS-08, and TMS-09 are shown in Fig. 7, while all the parameters obtained are summarized in Table 2.  $M_{rs}/M_s$  is a sensitive indicator of the magnetization state, which can give the distribution of magnetite domain state. If the sample contains only single domain (SD) particles of magnetite,  $M_{rs}/M_s$  equals to

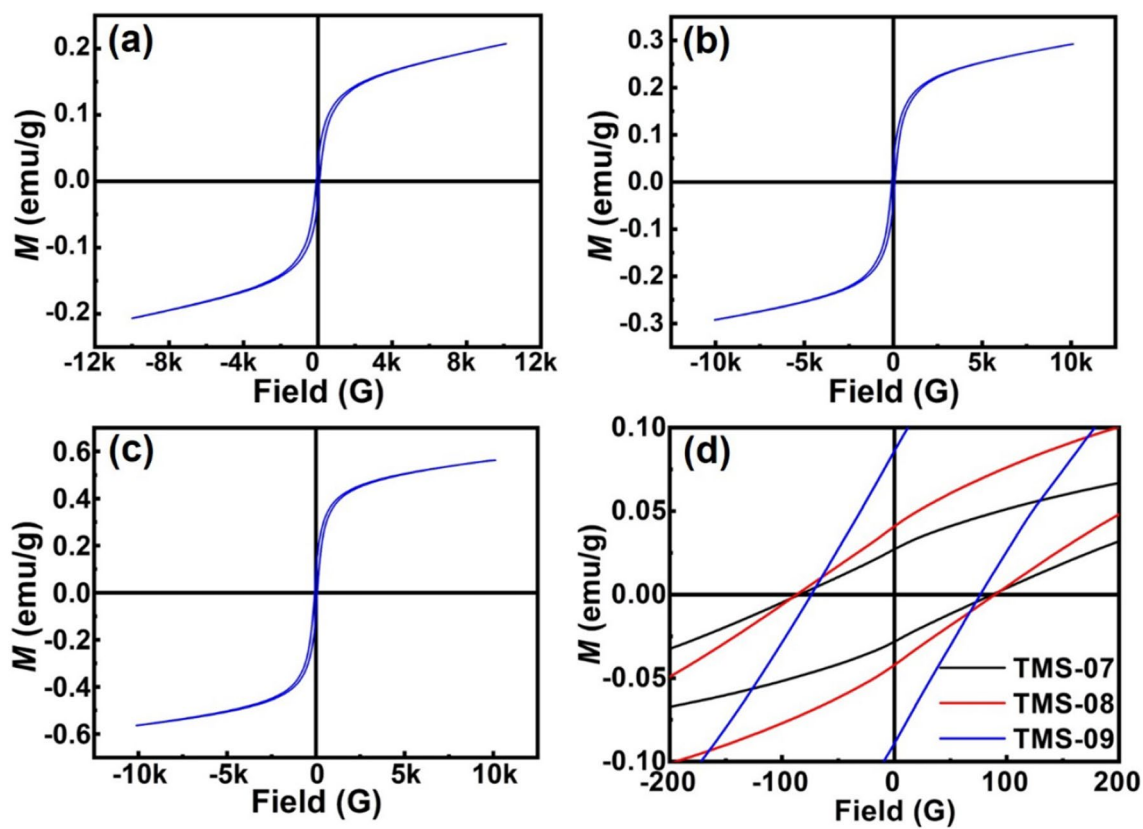


**Fig. 7** Hysteresis curves (a–c) and the enlarged image (d) of TMS-07, TMS-08, and TMS-09

**Table 2** Hysteresis parameters of TMS-07, TMS-08, and TMS-09

Sample No	$M_s$ (Am <sup>2</sup> /kg)	$M_{rs}$ (Am <sup>2</sup> /kg)	$B_c$ (mT)	$M_{rs}/M_s$
TMS-07	0.207	0.0276	91.2	0.133
TMS-08	0.292	0.0426	82.2	0.146
TMS-09	0.563	0.09	73.4	0.160

0.5. If the sample contains only multi-domain (MD) particles,  $M_{rs}/M_s$  is less than 0.1. And if there are only superparamagnetism (SP) particles in the sample,  $M_{rs}/M_s$  is 0 [22, 23].

From Table 2, the  $M_{rs}/M_s$  values of the samples were between 0.1 and 0.5, indicating that there were stable SD, MD, and SP particles in the magnetite. When the applied magnetic field was about 300 mT, the hysteresis loop was closed, and the sample reached saturation magnetization. It showed that the ferrimagnetic content was the main magnetic carrier mineral. At the same time, the slight “bee waist” morphology also manifested that the sample contained a small amount of antiferromagnetic minerals (SD + SP/MD). Different magnetic minerals have different residual magnetic flux

densities ( $B_r$ ). The  $B_r$  of soft magnetic minerals such as magnetite and maghemite is smaller, while that of hard magnetic minerals (hematite, goethite, etc.) is larger [24]. According to Fig. 6d,  $B_r$  values were similar and small as a whole, illustrating that soft magnetic minerals accounted for the main component in the samples.

The micro-Raman spectra of TMS-07, TMS-08, and TMS-09 are shown in Fig. 8. The brown-yellow and translucent bulk crystals were identified as quartz and feldspar by Raman spectra, respectively [25, 26]. By comparison, the peak intensities of TMS-09 were stronger than that of TMS-07 and TMS-08. In addition, the black lamellar crystals and reddish-brown reniform crystals only in TMS-09 were identified, as magnetite and hematite by Raman spectra. The Raman characteristic peaks of iron-containing minerals such as magnetite and hematite were not detected in TMS-07 and TMS-08. The overall intensity of Raman characteristic peaks was very weak, and even some are invisible. It can also reflect the firing temperature of pottery based on the intensity of Raman peaks. In consequence, it can be inferred that the firing temperature of TMS-09 is higher than that of TMS-07 and TMS-08, which is consistent with the results of XRD analysis. Meanwhile, TMS-07, TMS-08, and TMS-09

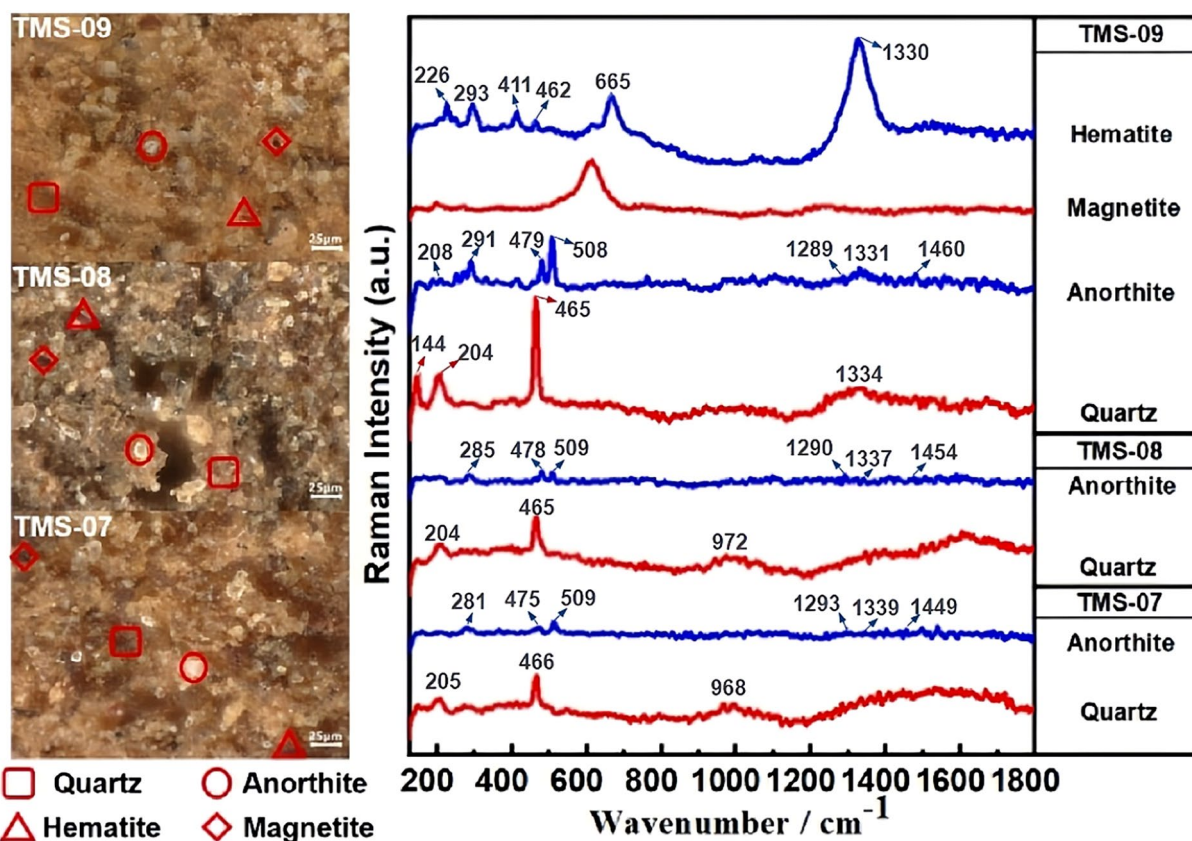


**Fig. 8** Optical micrographs under  $\times 1000$  and Raman spectra of TMS-07, TMS-08, and TMS-09

contain anorthite by comparing peak positions, which is also consistent with the XRD results.

Whether in ancient China or ancient Western countries, most of the clay as raw materials used for pottery production comes from near the kiln site, which is the essential reason for the differentiation of pottery characteristics in different regions [27, 28]. Yaozhou kiln was an essential kiln for firing pottery and porcelain in the Tang Dynasty. Its kiln scale and output were the largest in the north [29]. Therefore, the plain pottery excavated from the Tang Dynasty tomb of Liu Jing was most probably produced in Yaozhou kiln. The loess from Yaozhou kiln site was used as raw material to reproduce the plain pottery excavated in the Tang

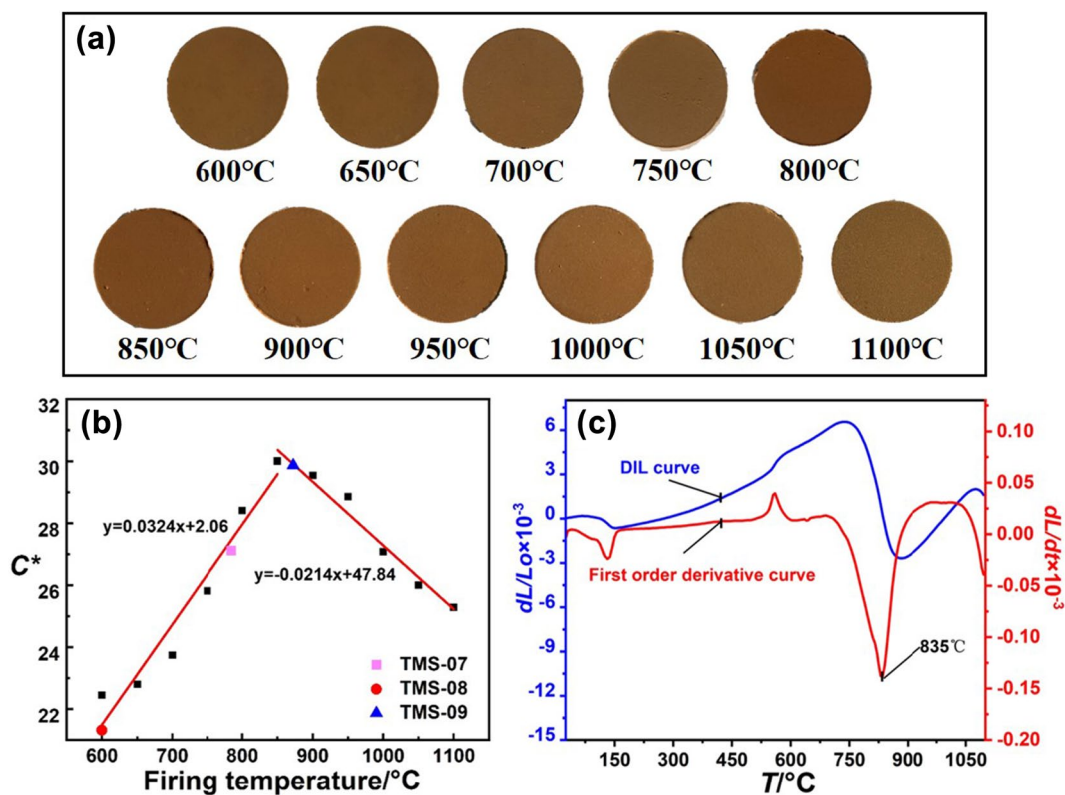
Dynasty tomb of Liu Jing. Its chemical composition is shown in Table 3. The loess was ground by mortar, sieved by a 40-mesh sieve, and granulated with 5 wt% moisture content. To obtain a cake-like body of  $\phi$  2 cm, the powder was pressed by a tablet press under 7 MPa for 15 s. Finally, the green bodies were fired by a muffle furnace at 600–1100 °C under an oxidizing atmosphere. The samples were heated from room temperature to 300 °C at 5 °C min<sup>-1</sup>, then to the target temperature at 3 °C min<sup>-1</sup>, and finally cooled naturally to room temperature in the muffle furnace.

Figure 9a is photos of replicas at different firing temperatures. It can be seen that the surface color of replicas is brownish-yellow, but the color saturation is varied.

**Table 3** Chemical composition of the loess from Yaozhou kiln site (wt%)

Sample	Na <sub>2</sub> O	MgO	Al <sub>2</sub> O <sub>3</sub>	SiO <sub>2</sub>	K <sub>2</sub> O	CaO	TiO <sub>2</sub>	Fe <sub>2</sub> O <sub>3</sub>
Loess	0.55 (0.04)	1.85 (0.12)	15.51 (0.29)	65.69 (0.77)	2.59 (0.20)	9.11 (0.50)	0.52 (0.23)	4.19 (0.84)

The value in the bracket is the standard deviation which is calculated by ten points of the loess from Yaozhou kiln site



**Fig. 9** Photos (a) and firing-temperature dependence of  $C^*$  of replicas at different firing temperatures (b) and thermal expansion curves of replicas fired at 600 °C (c)

Color saturation values on the surfaces of replicas were measured, as shown in Additional file 1: Table S3. Based on these data, the firing-temperature dependence of  $C^*$  for replicas is shown in Fig. 9b. Each plot was fitted using the least-squares method. The value of 0.92 for the coefficient of determination  $R^2$  indicated a strong correlation. From the calibration curve, with the increase of firing temperature,  $C^*$  value increased firstly and then decreased. Specifically, about 850 °C corresponding to the peak value was the glass phase formation temperature [6]. Based on the thermal expansion curve of the replicas fired at 600 °C (Fig. 9c), the glass phase formation temperature was 835 °C. Before the appearance of the glass phase, iron-containing minerals played a significant role in coloring. After the glass phase formation temperature, iron-containing minerals gradually dissolved in the glass phase, and iron ions in the glass phase and high purity iron crystallization in the body rose the vital function of coloring. It can also be seen from Fig. 9c that the net shrinkage temperature (the inflection point temperature) of the thermal expansion curve does not correspond to the original firing temperature for pottery whose firing temperature is lower than the glass phase formation temperature. The inflection point temperatures of the

thermal expansion curve corresponding to the sample under different heating rates cannot be determined the original firing temperature (Additional file 1: Fig. S2). In addition, the  $C^*$  at 27.12, 21.33, and 29.88 for TMS-07, TMS-08, and TMS-09 corresponded to a firing temperature of 773.5, 594.8, and 858.6 °C according to the calibration curve, which was consistent with XRD results. Furthermore, the color saturation values of thirty-two plain pottery fragments were substituted into the fitted  $C^*-T$  correlation curve, their firing temperatures were thus deduced, as shown in Table 4. Because the error of estimated firing temperature based on the fitted  $C^*-T$  correlation curves is large, the  $T$  values are rounded to the tens place. Therefore, the firing temperature of the ancient plain pottery could be estimated from the change in  $C^*$ .

It is worth noting that one color saturation  $C^*$  corresponds to two firing temperatures at the same time in the  $C^*-T$  correlation curve. However, the firing period of pottery can be roughly judged according to the epitaph in the unearthened tombs. At the same time, there is also a basic judgment on whether the pottery belongs to low-temperature or high-temperature pottery according to the appearance and surface hardness of the unearthened

**Table 4** The firing temperature determination of thirty-two plain pottery fragments by the color measurement

Sample	TY-01	TY-02	TY-03	TY-04	TY-05	TY-06	TY-07	TY-08
$C^*$	29.22	28.05	22.27	30.17	22.74	26.80	28.25	21.22
$T$ (°C)	840	800	620	870	640	760	810	590
Sample	TY-09	TMT-01	TMT-02	TMT-03	TMT-04	TMT-05	TMT-06	TMT-07
$C^*$	25.69	26.82	31.68	24.56	23.13	25.79	24.04	30.90
$T$ (°C)	730	760	910	690	650	730	680	890
Sample	TMT-08	TMT-09	TMT-10	TMT-11	TMT-12	TMS-01	TMS-02	TMS-03
$C^*$	25.20	29.32	33.41	28.69	28.10	29.62	29.99	23.89
$T$ (°C)	710	840	970	820	800	850	860	670
Sample	TMS-04	TMS-05	TMS-06	TMS-07	TMS-08	TMS-9	TMS-10	TMS-11
$C^*$	31.21	28.20	29.90	27.12	21.33	29.88	31.04	29.44
$T$ (°C)	900	810	860	770	590	860	890	850

pottery, so as to determine the firing temperature of pottery.

In addition, in order to verify the correlation and reliability of  $C^*-T$ , the loess near the eastern mausoleum of Qin Dynasty in Shaanxi Province was selected as the raw material, and pressed into cake-like bodies of  $\phi$  20 mm. The green bodies were fired at 600, 650, 700, 750, 800, 850, 900, 950, 1000, 1050, and 1100 °C under an oxidizing atmosphere. The color saturation  $C^*$  values of the samples were measured successively, and the results are shown in Additional file 1: Table S3. Similar to Fig. 9b, the measured data were fitted with the least square method to obtain the  $C^*-T$  correlation curve (Additional file 1: Fig. S3). It can be seen that the variation rule is consistent with the results obtained from the loess of Yaozhou kiln site, which further verifies the reliability of the determination of the firing temperature for plain pottery by the color measurement. The standard deviation and error of the estimated firing temperatures of the samples fired by the loess from Yaozhou kiln site and the eastern mausoleum of Qin Dynasty in Shaanxi Province are shown in Additional file 1: Table S4 and S5. It is found that the error of the firing temperature estimated by the color measurement is small, which indicates that this is an ideal method to measure the firing temperature of pottery, especially low-temperature plain pottery.

## Conclusions

Herein, for the plain pottery fragments excavated from the Tang Dynasty tomb of Liu Jing, the difference in  $C^*$  was not caused by the  $Fe_2O_3$  and  $TiO_2$  contents, humic acids in clay and the firing atmosphere, but was closely related to the firing temperature. The XRD, hysteresis loop, and Raman results showed that the plain pottery fragments contained a large amount of quartz and

feldspar crystals, as well as a small amount of mica mineral, magnetite, and hematite crystals. In order to study the intrinsic relationship between color and firing temperature, the plain pottery replicas were prepared by the loess from Yaozhou kiln site and the eastern mausoleum of Qin Dynasty in Shaanxi Province. The correlation between color saturation  $C^*$  and firing temperature  $T$  was established. The ancient firing temperatures of TMS-07, TMS-08, and TMS-09 were deduced by the fitted  $C^*-T$  correlation curve, and the results were in agreement with XRD, optical micrographs, and mercury intrusion data. In addition, the color saturation values of thirty-two plain pottery fragments were also measured and substituted into the fitted  $C^*-T$  correlation curve, their firing temperatures were thus deduced. The correlation between  $C^*$  and  $T$  can be explained as follows: The inflection point of the fitted  $C^*-T$  curve corresponded to the glass phase formation temperature, and the coloring mechanism is different before and after the inflection point. Before the appearance of the glass phase, iron-containing minerals played a vital role in coloring, and after the glass phase formation temperature, iron-containing minerals gradually dissolved in the glass phase, and iron ions in the glass phase and high-purity iron crystallization in the body rose the vital function of coloring. It is demonstrated that the color measurement is an ideal method for deducing the firing temperatures of ancient plain pottery by comparing the estimated firing temperatures obtained by the fitted  $C^*-T$  correlation curve with the known firing temperature of replicas. It would eliminate the hassle of sample preparation and estimation of the firing temperatures with the nondestructive style. This method could be useful for both archaeology and cultural relics conservation science.

## Supplementary Information

The online version contains supplementary material available at <https://doi.org/10.1186/s40494-024-01178-5>.

**Additional file 1: Table S1.** Chroma values on the surfaces of thirty-two plain pottery fragments. **Table S2.** Chemical compositions obtained by XRF on the surfaces of thirty-two plain pottery fragments (wt%). **Table S3.** Color saturation values on the surfaces of replicas. **Table S4.** The standard deviation and error of the estimated firing temperatures of the samples fired by the loess from Yaozhou kiln site. **Table S5.** The standard deviation and error of the estimated firing temperatures of the samples fired by the eastern mausoleum of Qin Dynasty in Shaanxi Province. **Fig S1.** Porosity and average pore size of MS-07, TMS-08 and, TMS-09. **Fig S2.** Thermal expansion curves and the first order derivative curves of replicas fired at 600 °C with 3, 5, and 10 °C/min, respectively. **Fig S3.** The  $C^* - T$  correlation curve of the samples fired by the loess near the eastern mausoleum of Qin Dynasty in Shaanxi Province.

### Acknowledgements

Not applicable.

### Author contributions

ZXC and LDY provided experimental samples. SP, ZJF, LHJ and WF defined the research project and designed the experiments. ZB, WH and HXL carried out the experiments. ZB, WH, HXL, FGQ and SP performed the analyses. ZB and SP wrote the first draft manuscript and all co-authors discussed the results and commented on the manuscript. All authors reviewed, edited the final manuscript. All authors read and approved the final manuscript.

### Funding

This work was supported by the National Natural Science Foundation of China (No. 52102108, No. 52102026, and No. 52272019), Postdoctoral Research Foundation of China (No. 2021M691997), Silicate Cultural Heritage Protection and Utilization Innovation Team of Shaanxi Province (No. 2020TD-008), Foreign Expert Service Program Project of Shaanxi Province (No. 2023WGZJ-YB-06) and Key Scientific Research Program of Shaanxi Province Education Department (No. 22JY009 and No. 22JY010).

### Availability of data and materials

All data generated or analyzed during this study are included in this published article.

### Declarations

### Competing interests

The authors declare that they have no competing interests.

Received: 24 May 2023 Accepted: 9 February 2024

Published online: 19 February 2024

## References

- El-Gohary M, El-Ghareb W, Saad M. Damage quantification of archaeological pottery in Sheikh Hamad "Athribis" Sohag-Egypt. *Ceram Int*. 2019;45(14):17611–9.
- Li XX, Yu WD, Lan DS, Zhao J, Huang JH, Xi N, Li Q, Xia Y, Zhou P, Luo HJ. Analysis of newly discovered substances on the vulnerable Emperor Qin Shihuang's Terracotta Army figures. *Herit Sci*. 2022;10(1):72.
- Müller NS, Vekinis G, Day PM, Kilikoglou V. The influence of micro-structure and texture on the mechanical properties of rock tempered archaeological ceramics. *J Eur Ceram Soc*. 2015;35(2):831–43.
- Nijjima S, Taniguchi H, Murate K, Kawase K. Terahertz spectroscopy applied to estimation of firing temperatures of ancient ceramics. *IEEE Thz Sci Techn*. 2022;12(3):300–6.
- Roberts JP. Determination of the firing temperature of ancient ceramics by measurement of thermal expansion. *Archaeometry*. 1963;6(1):21–5.
- Tong YD, Wang CM. Application and exploration of the thermal expansion technology in determination of the firing temperature of ancient ceramic. *J Guangxi Univ Natl*. 2017;23(3):33–9.
- Tite MS. Determination of the firing temperature of ancient ceramics by measurement of thermal expansion: a reassessment. *Archaeometry*. 1969;11:131–43.
- Lu XK, Xu CS, Li WD. Applied research on the push-rod thermal expansion method used to determine firing temperatures of ancient ceramics. *Sci Conserv Archaeol*. 2020;32(11):70–80.
- Moon DH, Kim SJ, Nam SW, Cho HG. X-ray diffraction analysis of clay particles in ancient Baekje black pottery: indicator of the firing parameters. *Minerals*. 2021;11(11):1239.
- Palanivel R, Kumar UR. Thermal and spectroscopic analysis of ancient potteries. *J Therm Anal Calorim*. 2011;56(1–2):195–208.
- Bruni S. Etruscan fine ware pottery: near-infrared (NIR) spectroscopy as a tool for the investigation of clay firing temperature and atmosphere. *Minerals*. 2022;12(4):412.
- Chazhengina SY, Summanen IM, Svetov SA. Raman spectroscopy for firing condition characterization: case study of Karelian medieval pottery. *J Raman Spectrosc*. 2020;51(9):1894–902.
- Mirti P. On the use of colour coordinates to evaluate firing temperatures of ancient pottery. *Archaeometry*. 1998;40(1):45–57.
- Mirti P, Davit P. New developments in the study of ancient pottery by colour measurement. *J Archaeol Sci*. 2004;31(6):741–51.
- Shi P, Wang F, Zhang B, Luo HJ, Zhu JF, Fei GQ. Study on the coloring mechanism of the Ru celadon glaze in the Northern Song Dynasty. *Ceram Int*. 2020;46(15):23662–8.
- Rella S, De Benedetto GE, Marchetta I, Malitesta C. Provenancing of VI–VII century terra sigillata coming from Matera burial area by X-ray photoelectron spectroscopy. *J Cult Herit*. 2016;17:194–7.
- Demirci S, Yurddaskal M, Dikici T, Sarioglu C. Fabrication and characterization of novel iodine doped hollow and mesoporous hematite (Fe<sub>2</sub>O<sub>3</sub>) particles derived from sol-gel method and their photocatalytic performances. *J Hazard Mater*. 2018;345:27–37.
- Colomban P. Chemical preparation routes and lowering the sintering temperature of ceramics. *Ceramics*. 2020;3:312–39.
- Montecchio D, Francioso O, Carletti P, Pizzeghello D, Chersich S, Previtali F, Nardi S. Thermal analysis (TG-DTA) and drift spectroscopy applied to investigate the evolution of humic acids in forest soil at different vegetation stages. *J Therm Anal Calorim*. 2006;83(2):393–9.
- Boguta P, Sokolowska Z, Skic K. Use of thermal analysis coupled with differential scanning calorimetry, quadrupole mass spectrometry and infrared spectroscopy (TG-DSC-QMS-FTIR) to monitor chemical properties and thermal stability of fulvic and humic acids. *PLoS ONE*. 2017;12:e0189653.
- Papadopoulou DN, Lalia-Kantouri M, Kantiranis N, Stratis JA. Thermal and mineralogical contribution to the ancient ceramics and natural clays characterization. *J Therm Anal Calorim*. 2006;84:39–45.
- Jordanova N, Jordanova D, Barrón V, Lesigyrski D, Kostadinova-Avramova M. Rock-magnetic and color characteristics of archaeological samples from burnt clay from destructions and ceramics in relation to their firing temperature. *Archaeol Anthropol Sci*. 2019;11(7):3595–612.
- Li X, Wu YJ, Mao LJ, Wu XT, Song YB. Determination of the thermal temperatures of burnt clay at Sujiaocun site based on magnetic susceptibility. *Sci Conserv Archaeol*. 2022;34(1):63–70.
- Huang XG. Preliminary rock magnetic study of archaeomagnetic samples. *Chin J Geophys*. 1999;42(5):660–8.
- Wang T, Chen P, Wang ML, Sang Z, Zhang P, Wang F, Sciau P. Micro-structural study of Yaozhou celadons (Tang to Yuan Dynasty): probing crystalline and glassy phases. *J Eur Ceram Soc*. 2020;40(13):4676–83.
- Castagnaro IB, Nucera A, Barberi RC, Castriota M. Study and micro-Raman characterization of pigments present on majolicas of historical and artistic interest from Gerace, Italy. *Herit Sci*. 2023;11(1):24.
- Milosevic M, Logar M, Djordjevic B. Mineralogical analysis of a clay body from Zlakusa, Serbia, used in the manufacture of traditional pottery. *Clay Miner*. 2020;55(2):142–9.

28. Rathossi C, Pontikes Y. Effect of firing temperature and atmosphere on ceramics made of NW Peloponnese clay sediments. Part I: reaction paths, crystalline phases, microstructure and colour. *J Eur Ceram Soc.* 2010;30(9):1841–51.
29. Wang XM. Technological characteristics, origin and influence of the raw body black color porcelain of Yaozhou kiln in Tang Dynasty. *Archaeol Cult Relics.* 2013;3:73–9.

### **Publisher's Note**

Springer Nature remains neutral with regard to jurisdictional claims in published maps and institutional affiliations.